Inclination Angle Effect and Separation Zones Estimation for Incompressible Flows inside Pipes using Sub-Grids Refinement

CHRISTINA G. GEORGANTOPOULOU
School of Engineering, Bahrain Polytechnic
Isa Town, Po box 33349
KINGDOM OF BAHRAIN
Christina@polytechnic.bh

Abstract: - The particular characteristics of flows inside channels present high interest to the industrial sector concerning pipes design, construction, corrosion and control issues. In the present paper the numerical estimation and investigation of incompressible viscous flows inside inclined step pipes are approached trying to produce accurate flow variables results and certain data concerning the separation zones and the inclination angle effect according to the various Reynolds numbers values. Cartesian grids are generated for the domain discretization in combination with a block-nested refinement technique, trying to avoid the huge computational memory is needed when the aspect ratio of the physical domain is high enough. The angle effect is investigated concerning the recirculation zones and the energy flow losses, trying to predict the optimum geometrical selection of pipes related to the flow rate, hydraulic diameter and inclination angle. The Navier – Stokes equations are solved using an artificial compressibility method in combination with upwind numerical schemes. Various results are presented for several grid sizes and Reynolds numbers for four different inclination step angles. It seems that this flow is characterized by extended recirculation zones even at low Reynolds numbers, but using the appropriate step angle according to the flow rates values the energy losses can be minimized.

Key-words: - flow in pipes, inclination angle, block nested grids, recirculation, numerical estimation

1 Introduction

The sudden expansion pipes are extensively used in the industrial sector as in power plants, aluminium production processes or oil and gas companies. The relationship among the width and the inclination angle of the channel is quite important in order the recirculation areas as well as the major energy losses to be avoided. In this paper the numerical investigation of this issue is developed, trying to produce a computational model and flexible tool for industrial applications.

Such tools are quite useful for related applications and several proposed methods have already been developed. Interesting approaches for sudden expansion channels can be found at Lee [1] and Santos [2] work, where emphasis is given not only to the computational estimation of the flow but also to the experimental validation of the results [3, 4]. By the other hand some important numerical results concerning the aforementioned flow simulation in channels has been presented by Louda [5, 6], who applies a finite element method producing quite satisfied accuracy focusing at the recirculation zones' location [7]. Pressure behavior is analyzed extensively by Razani [8], while a three dimensional approach is presented by Kaiktsis [9]. Wallin [10], develops an explicit methodology and present flow variables results for high Reynolds numbers flows which is applied quite satisfactory for the sudden expansion channels flow simulation and computation [11].

However the numerical simulation and estimation of flows for industrial pipe flow applications, according to our research, shouldn't be only accurate and independent according to the flow conditions, but also, simple, flexible and easily adaptable for any pipe flow application. In all the above approaches, quite important flow information is presented, although lack of specific details exists concerning the inclination angle effect to the developing flows in order to present useful conclusions and technical advices for

numerous industrial applications. By the other hand in most of the cases, the refinement technique which is applied is quite efficient but not so simple and flexible in order to be easily adapted in every individual industrial case. In most of the cases hybrid adapted grids are generated in order to overcome the incline edge of the sudden expansion channels and a local adaptive refinement technique is developed in order to provide better accuracy at the crucial flow areas. However Cartesian grids present better flexibility and support as well as easy discretization of the governing equations, if of course the geometry description allows to be applied. Corrier [12] has presented a quite flexible Cartesian grid scheme, which can be independent by the geometrical bound and produces accurate flow results, while similar approaches develop techniques based on approximated bounds creation using only grid lines in order to describe the flow domain [13]. Apparently, the uniform Cartesian grid generation cannot be satisfied when geometries with high aspect ratios are simulated. Interesting refinement techniques have been presented by Wang [14], where a quadrilateral grid generator is presented based on cell cutting [15, 16], while in Pan's approach [17], a ghost cells method for incompressible flows is developed promising a flexible scheme for channels' flows. Even in finite elements methodology the adaptive refinement techniques promise high accuracy achieving reduction of the computational memory simultaneously [18].

1.1 Aim and objectives

The inclination angle effect and the location of the separation zones inside sudden expansion channels are numerically investigated in the present paper. In addition main objective of our work is not only the extended calculation and presentation of the related flow results, but also the development of a flexible, simple and easy to be applied computational scheme, adaptable to any relating industrial application. In order to achieve the physical domain discretization, Cartesian grid methodology is developed using only grid lines, which can be applied for every channel geometry domain [19]. This method is based on an initial approach of Tseng [20], while it has been already applied successfully for pipe flows prediction in our recent research work [21]. Refinement technique will be developed based on block nested sub-grids sequence at the crucial areas of the geometry, using various refinement factor values and grid levels [22, 23]. Flux vector splitting methodology in combination with the artificial compressibility technique will be used for the Navier-Stokes equation solution [24], an accurate scheme which has been previously applied in various internal and external flows numerical estimation. The scheme is cell-centered, using finite volume technique, while special treatment will be presented concerning the boundary conditions application among the various types of domain interfaces after the grid generation [25]. Numerical calculations will be analyzed for three different inclination angles of the pipe and for various Reynolds number values trying to predict the relationship of the step angle with the recirculation zones, the energy losses and the flow characteristics, as well as the grid independence and the accepted accuracy of the block nested refinement technique. Validation of the results is performed using the corresponded ones by the literature as well as by commercial numerical software.

2 Theoretical Analysis And Numerical Methodology

The mathematical modeling is comprised of three main sections; the grid generation technique, the exploitation and application of the boundary conditions and finally the numerical solution of the governing equations. However, due to the block nested refinement technique, a special treatment is needed concerning the boundary conditions application, according to the type of each physical domain bound and the location of each sub-grid.

2.1 Cartesian grid approach

Concerning the numerical estimation of flows inside pipes, the Cartesian grids are more appropriate, although non - Cartesian bounds are met according to the channels' shape. At the flow case of the inclined step pipes, there is only one non-Cartesian bound, which is not enough to force the hybrid grids development and usage as some of the researchers prefer [5], although the accuracy of the results is very satisfied and acceptable. In our method all the geometry bounds are laid on Cartesian grid lines and consequently in order to succeed it, an approximated bound close as possible to the original one is produced. The initial description of the geometry is achieved by a set of data points, which are used in

combination with the rule of minimum distance in order to produce the new approximated data ones (fig. 1). All the new points, which have been extracted by this procedure, are grid nodes and these are connected using straight grid lines, applying the saw-tooth method. For the case of inclined step pipes, only one bound is non-Cartesian, which will be re-generated using the above method as we can see at Fig. 2. More details about this technique can be found in our previous research work [21, 25].

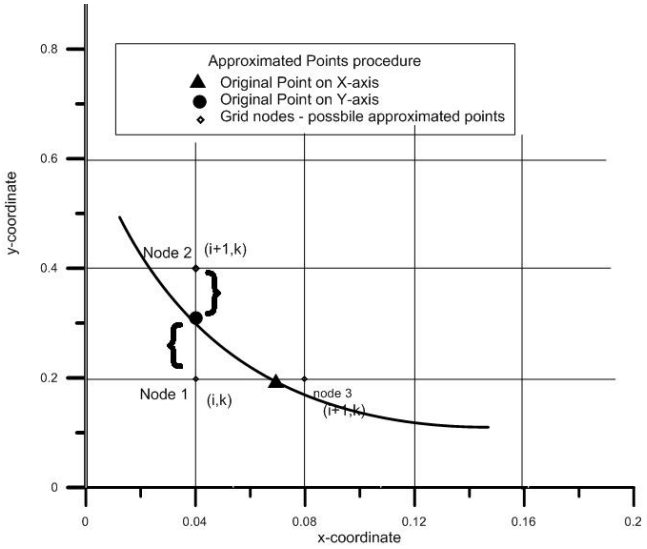

Fig. 1. Approximated points definition and procedure

In order to overcome issues concerning the high aspect ratios, which are presented in all the pipes' structures, a refinement technique is necessary to be applied in order to reduce the computational time and memory and achieve the desired accuracy simultaneously. The refinement technique which has been chosen is a block - nested methodology by the use of a hierarchical structured grid approach. The method is based on using a sequence of nested rectangular meshes in which numerical simulation is taking place (Fig. 3). The whole domain is a rectangle, whose sides lie in the coordinate directions, except for the case of the inclined step outer bound. Concerning the inclined domain location, only three edges are straight lines, while the fourth edge is a crooked one, due to the used approximation technique. We simulate the domain based on as many refine grids as we need according to the flow domain demands [25]. The proposed nested algorithm contains several levels of grids. We name the coarsest level *l=0* and each next refine sub – grid is named *l+1*. We define the integer refinement factor *I*, as follows:

$$I = dx_m / dx_{m+1} = dz_m / dz_{m+1}. \qquad (1)$$

where I is the refinement factor, dx_m *and* dx_{m+1} the grid's resolution in longitude for the m grid level and for the $m+1$ (next) grid level, respectively, while dz_m *and* dz_{m+1} the grid's resolution in latitude for the grid levels as above. The I is always a power of two, while the choice of the location for the nested grids is usually decided according to the velocity differences among the adjacent cells.

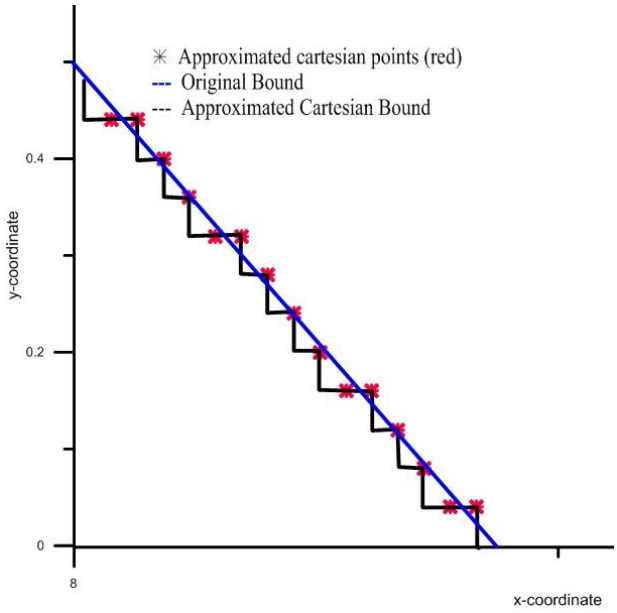

Fig. 2. Connection method (saw-tooth) for the approximated points at the inclined step bound.

2.2 Governing equations & numerical scheme

In order to numerical calculate the incompressible flow along the pipes we solve the system of the Navier – Stokes equations in combination with the mass conservation one. The N-S equations in Cartesian coordinates, two dimensional can be seen below:

$$\frac{\partial \rho}{\partial t} + \frac{\partial (\rho u)}{\partial x} + \frac{\partial (rw)}{\partial z} = 0 \ (2)$$

$$[\Gamma]\frac{\partial q}{\partial t} + \frac{\partial e}{\partial x} + \frac{\partial g}{\partial z} = \frac{1}{\mathrm{Re}}\left(\frac{\partial r}{\partial x} + \frac{\partial s}{\partial z}\right) (3)$$

$$[\Gamma]\frac{\partial q}{\partial t}+\frac{\partial e}{\partial x}+\frac{\partial g}{\partial z}+\alpha\cdot\frac{g_1}{z}=\frac{1}{Re}\left(\frac{\partial r}{\partial x}+\frac{\partial s}{\partial z}+\alpha\cdot\frac{s_1}{z}\right) \quad (4)$$

where,

$$[\Gamma]=\mathrm{diag}\left(\frac{1}{\beta},1,1\right)^{T} \quad (5)$$

after the addition of the artificial compressibility term β, a is a switch for the activation of the axisymmetric terms ($\alpha=0$ is non axisymmetric, $a=1$ axisymmetric flow field), Re the Reynolds number and Q the unknown solution vector, as follows:

$$Q=(p\ \ u\ \ w)^{T} \quad (6)$$

with p being the pressure, and $(u,\ w)$ the velocity components in physical space, e, g, g_1 and r, s, s_1 are respectively the convective and diffusive flux vectors at the plane (x, z).

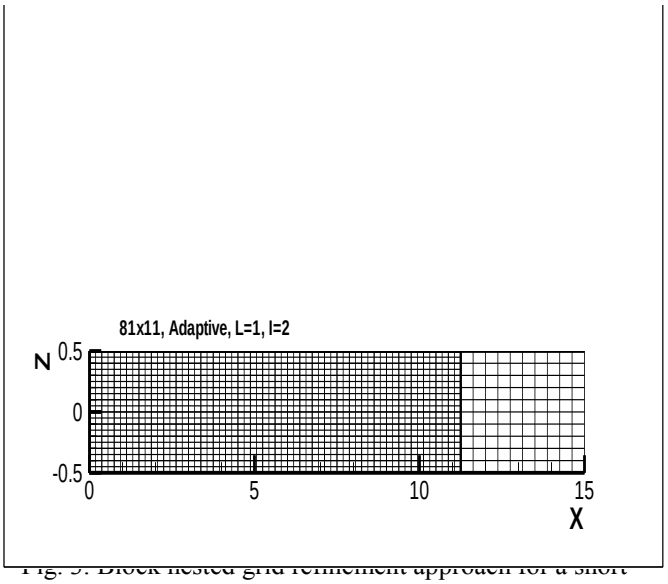

Fig. 3. Block nested grid refinement approach for a short pipe, based grid size: 81x11, one (1) and two (2) levels of refinement and integer refinement factor equal to two (2).

In order to avoid the lack of the pressure term by the unknown solution vector, we introduce the artificial compressibility term β and by this way we achieve the connection among the convective flux vectors and the unknown flow variables vector Q. We could probably introduce one more equation in order to calculate the pressure, but this would forbid the implicit scheme development [24].

Apparently, the above N-S equations are the governing equations for unsteady flows, although we will study and estimate only steady flows in the present research work. However, this form of the equations can be used for the solution of steady flow fields as in our case as we know that these are non-linear and iterative method are needed for their solution. In these steady cases the time derivative is used for the construction of an iterative technique using the artificial time step ∂t in order to define the final steady state. Here, we extend the Flux vector splitting (FVS) method for solving incompressible flow fields implicitly. In such flow fields the splitting of the convective flux vectors has to change sense because of their non-homogeneous property. The values of the flux vectors at the cell faces are approached by upwind schemes up to third order of accuracy. The un-factored discretized Navier-Stokes equations are solved by an implicit second order accurate in time scheme, using Gauss-Seidel relaxation technique.[27] The finite-volume methodology is applied, cell centered, while the value of the β term is usually equal to the reference velocity.

2.3 Boundary conditions

Special treatment of the boundary conditions is needed due to the block nested grid algorithm development. The conditions which are appropriate to be applied are related to the type of the interface that is met during the numerical solution of the flow equations.

2.3.1 Boundaries at the physical bounds

The boundaries at the physical bounds are either Dirichlet either Neumann conditions, according to the bound nature, as these can be seen at the below Table 1 with reference to Fig. 4, where u *and* w are the velocity components, p the pressure and the indicator *ref* shows the reference values of the field.

The method which is applied in our approach is a finite volume methodology which in the case of the 2-D Cartesian grids is almost similar with the finite difference one. According to the location of each bound, backward or forward differences are applied in order to set the appropriate conditions. Similar approaches successfully have been developed in pipe simulation in our previous research work or even in numerical schemes with other various applications [26,27].

Table 1: Boundary conditions for the inclined step pipe (Fig. 4)

Geometry Bounds (Fig. 4)	**Boundary Conditions**
AB	Inlet conditions $u = u_{ref}$, $w = 0, \frac{\partial p}{\partial x} = 0$
AC	No slip condition (wall) $u = w = 0, \frac{\partial p}{\partial z} = 0$
CD	No slip condition (wall) $u = w = 0, \frac{\partial p}{\partial z} = 0$
DE	No slip condition (wall) $u = w = 0, \frac{\partial p}{\partial z} = 0$
EF	Outlet $\frac{\partial u}{\partial x} = 0, w = 0, p = p_{ref}$
BF	No slip condition (wall) $u = w = 0, \frac{\partial p}{\partial z} = 0$

2.3.2 Boundaries among course – fine interfaces

At the initial steps of the block nested algorithm, the velocity values will be transferred from a coarse interface (grid level $= l_i$) to a refine one (grid level $l = l_{i+1}$). It is important to be mentioned that in this stage the artificial (ghost) cells are neglected:

$$u_{l,m} = u_{l,m+1} = u_{i,j} \quad (7)$$

where $u_{l,m}$ and $u_{l,m+1}$ are the axial velocity components at the refined grid level and $u_{i,j}$ the corresponded one at the coarse level. At the specific flow case study in various sub-grids domains, the vertical velocity component is equal to zero (0) and so this is set at the aforementioned boundaries. However, even if $\neq 0$, the values will be transferred by a similar way with the axial velocity components as above:

$$w_{l,m} = w_{l,m+1} = w_{i,j} \quad (8)$$

All the symbols are as these described above (paragraph 2.3.1).

2.3.3 Boundaries among fine – course interfaces

In the case that the boundary values must be transferred through fine – course interface the below formula is applied:

$$u_{i,j} = \frac{u_{l,m+1} + u_{l,m}}{2} \quad (9) \quad \text{and } w_{i,j} = \frac{w_{l,m+1} + w_{l,m}}{2} \quad (10)$$

where the values are as described above.

2.3.4 Boundaries among fine – fine interfaces

In some cases, according for example the location of the separation zones inside the pipe, fine grids are adjacent and the variables values have to be transferred among them. The level of the grids receives the same value in both of the sub-grids and the velocity values are given as it can be seen below:

$$u_{l,m} = u_{k,n} \qquad and \qquad w_{l,m} = w_{k,n} \quad (11)$$

2.3.5 Boundaries among course- course interfaces

As the aforementioned grid methodology is applied only for rectangular Cartesian grids and sub-grids, there are some cases that course grids will be adjacent and the related boundary conditions must be set in order the numerical calculation to take place. In that case the boundaries application is developed as at the above case fine-fine interface (Eq. 11).

3 Results and Discussion

The inclination angle effect is going to be investigated to the incompressible flow inside pipes as various industrial applications are based on this type of flow and pipe. In order to succeed that and manage to present accurate evidence about the flow characteristics, the Cartesian block nested technique will be applied with the appropriate choice of sub-grids and refinement levels as well, trying to reduce the CPU time, reduce the computational memory and keep the desired accuracy of our flow results. Consequently, validation data are presented in order to prove first of all the accuracy of the numerical scheme, as well as the efficiency of the block nested algorithm. By presenting the following extended analysis we attempt to enhance previous research work which has been done on the aforementioned

flow fields [3,28] and extend our research work in incompressible viscous flows inside pipes [19,29].

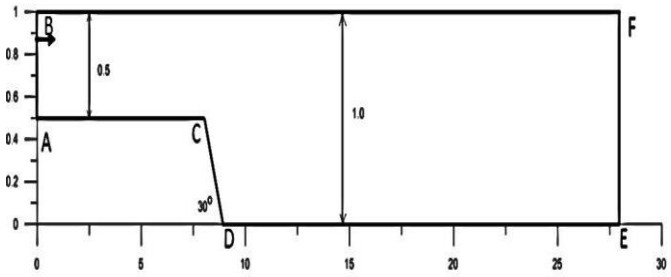

Fig. 4. Geometry description of the inclined step pipe. The dimensionless lengths of the channel vary according to the *Re* value.

3.1 Incline step pipe geometry

The geometry description and the related dimensions can be seen at the above Fig. 4.

The relevant height H_{ref} has set equal to 1 for dimensionless purposes and it is the maximum hydraulic diameter of the pipe. The inlet area receives $H_{ref}/2$ height as we study a sudden expansion pipe.

In order to investigate the inclination angle effect to the flow, we present various calculations for four (4) different inclination angles values: 10^o, 30^o , 45^o and 90^o (Fig. 5), for five different *Re* values: 100, 400, 800, 1200 and 1700. The numerical solution has taken place using uniforms and block nested grids one or two levels of refinement and various grid sizes in order to prove the grid independence of the final solution.

3.2 Recirculation lengths and points

The results that are presented have been produced using grid size 351x26, with two refinement grid levels and *I=2*. In all the cases the expansion ratio is set to be equal to 2 (Fig. 4). At the following tables the separation zones of the lower and the upper wall of the pipes are presented according to the inlet flow rate for the above *Re* values. Detachment and reattachment points have been located in order to provide even more efficient information concerning the exact location of the separation zones.

For validation purposes all the numerical cases solved using the commercial software ANSYS and two (2) of these are presented for inclination angle equal to 90 *deg* for all the range of the used *Re*, using uniform grid sized 651x26.

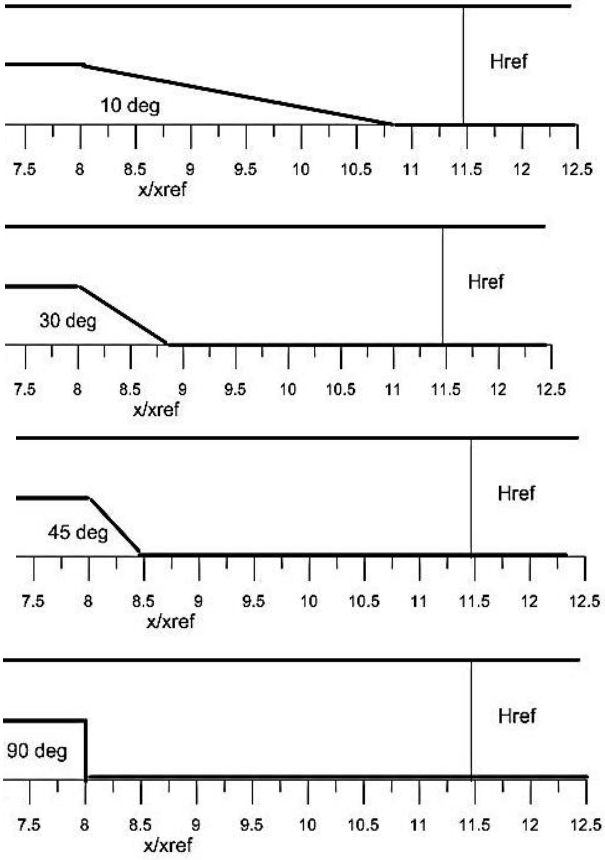

Fig. .5 Geometry description of the incline step pipe for different values of the inclination angle.

Table 2: Recirculation lengths and related points –lower wall: Inclination angle 10 *deg*. Grid, 351x13, *l=2, I=2.*

Re	Lower Wall		
	Recirculation Length	Detachment Point	Reattachment Point
100	No detection	No detection	No detection
400	No detection	No detection	No detection
800	No detection	No detection	No detection
1200	4.53	17.47	22.00
1700	8.07	18.71	26.78

In addition the present work results are compared with the corresponded ones by the literature where the convergence is accepted. The appropriate modifications have been performed in order to present the relating results according to the expansion

ratios which have been used in each case (Tables 8, 9).

Table 3: Recirculation lengths and related points –upper wall: Inclination angle 10 *deg*. Grid, 351x13, *l*=2, *I*=2.

Re	**Upper Wall**		
	Recirculation Length	**Detachment Point**	**Reattachment Point**
100	No detection	No detection	No detection
400	No detection	No detection	No detection
800	4.57	8.85	16.34
1200	7.54	8.53	18.71
1700	10.28	8.48	19.68

Table 4: Recirculation lengths and related points – lower wall: Inclination angle 30 *deg*. Grid, 351x13, *l=2, I=2*.

Re	**Lower Wall**		
	Recirculation Length	**Detachment Point**	**Reattachment Point**
100	0.39	8.90	9.29
400	4.15	8.26	12.41
800	6.46	8.26	14.72
1200	7.56	8.26	15.91
1700	8.94	8.26	17.20

Table 5: Recirculation lengths and related points – lower wall: Inclination angle 30 *deg.* Grid, 351x13, *l=2, I=2*.

Re	**Upper Wall**		
	Recirculation Length	**Detachment Point**	**Reattachment Point**
100	No detection	No detection	No detection
400	No detection	No detection	No detection
800	4.74	13.54	18.28
1200	7.54	14.51	22.05
1700	10.07	15.85	25.92

Table 6: Recirculation lengths and related points – lower wall: Inclination angle 30 *deg,* ANSYS – Fluent, Cartesian uniform grid 651x26.

Re	**Lower Wall**		
	Recirculation Length	**Detachment Point**	**Reattachment Point**
100	0.44	8.89	9.33
400	4.28	8.28	12.56
800	6.58	8.28	14.86
1200	7.74	8.28	16.02
1700	9.03	8.28	17.31

Table 7: Recirculation lengths and related points – upper wall: Inclination angle 30 *deg*, ANSYS – Fluent, Cartesian uniform grid 651x26.

Re	**Upper Wall**		
	Recirculation Length	**Detachment Point**	**Reattachment Point**
100	No detection	No detection	No detection
400	No detection	No detection	No detection
800	5.02	13.55	18.57
1200	7.72	14.55	22.27
1700	10.13	15.93	26.06

Table 8: Recirculation lengths and related points – lower wall: Inclination angle 45 deg. Grid, 351x13, l=2, I=2.

Re		**Lower Wall**	
	Recirculation Length	**Detachment Point**	**Reattachment Point**
100	1.24	8.10	9.34
400	3.82	8.10	11.92
800	6.68	8.10	14.78
1200	8.99	8.10	17.09
1700	10.86	8.10	18.96

Table 9: Recirculation lengths and related points – upper wall: Inclination angle 45 deg. Grid, 351x13, l=2, I=2.

Re	**Upper Wall**		
	Recirculation Length	**Detachment Point**	**Reattachment Point**
100	No detection	No detection	No detection
400	1.78	11.49	13.27
800	4.20	13.81	18.01
1200	6.19	15.75	21.94
1700	8.72	17.20	25.92

As it is depicted by all the tables, there are mainly two separation zones the most, inside the channel ($Re < 1700$), while the recirculation at the upper wall cannot be detected when the *Re* is equal to 100 and 400 in most of the cases.

As the flow rate increases, the recirculation length increases as well as on both of the channel's walls. However, although the detachment points at the lower wall remain at the same position for all the inlet velocities (around 8.26 except for the case of *Re*=100), the one at the upper wall is moving forward according to the related Re. Despite of this fact the recirculation length at the upper bound is increased as the *Re* increases. For the value of *Re* equal to 100

although the separation zones are not so extended, it seems that there is a low width recirculation at the upper surface of the pipe, which, when the *Re* is equal to 1700, receives a significant value. However it seems to be reasonable according to the expansion ratio as well as to Fig. 8. In Tables 4 – 7 the related information is presented for the inclination angle value equal to 30 deg.

Table 10: Recirculation lengths and related points – lower wall: Inclination angle 90 deg. ANSYS – Fluent, Cartesian uniform grid 651x26.

Re	**Lower Wall**		
	Recirculation Length	**Detachment Point**	**Reattachment Point**
100	1.30	8.05	9.35
400	3.35	8.05	11.40
800	4.15	8.05	12.20
1200	5.25	8.05	13.30
1700	5.85	8.05	13.90

Table 11: Recirculation lengths and related points – upper wall: Inclination angle 90 deg. ANSYS – Fluent, Cartesian uniform grid 651x26.

Re	**Upper Wall**		
	Recirculation Length	**Detachment Point**	**Reattachment Point**
100	No detection	No detection	No detection
400	1.20	11.55	12.75
800	4.60	12.00	16.60
1200	6.80	12.60	19.40
1700	8.60	13.10	31.70

The numerical estimation has been developed using both of the computational techniques (block – Cartesian and ANSYS) for validation purposes, where the convergence of the results is acceptable, presenting very low relative error ($4 \times 10^{-3} < rel.error < 5.5 \times 10^{-3}$). It seems that the development of the recirculation in both of the pipe's walls is higher than the previous case (angle equal to 10 *deg)*, the detachment point of the lower wall remains in constant position and the upper wall separation zone is moving forward according to the Re.

Similar effects are depicted to the following tables (Tables 8 - 13), where all the recirculation zones data are presented with all the necessary details. The main findings by the above tables are that as you increase the flow rate, the expansion of the separation zones is increased as well. The relating recirculation data are presented for the present methodology and other corresponded by the literature in the following Tables 14 and 15 .

Table 12: Recirculation lengths and related points lower wall: Inclination angle 90 deg, grid 351x13, *l=2, I=2.*

Re	**Lower Wall**		
	Recirculation Length	**Detachment Point**	**Reattachment Point**
100	1.17	8.05	9.22
400	3.71	8.05	11.76
800	6.25	8.42	14.67
1200	7.53	8.45	15.98
1700	8.12	8.50	16.62

Table 13: Recirculation lengths and related points upper wall: Inclination angle 90 deg, grid 351x13, *l=2, I=2.*

Re	**Upper Wall**		
	Recirculation Length	**Detachment Point**	**Reattachment Point**
100	No detection	No detection	No detection
400	1.72	11.55	13.27
800	4.40	12.75	17.15
1200	6.75	15.15	21.90
1700	7.85	16.01	23.86

The present work numerical data have been retrieved by 351x13 grid size, *l=2* and *I=2.* It seems that the convergence is acceptable since the relative errors receive very low values. However in some cases, certain differences are depicted. These seem to be developed due to the different grid sizes, the different entrance pipe lengths or the differences to the outflow boundary conditions application.

Table 14: Recirculation zones data comparison among various methodologies through literature

Re 800	**Lower rec/ion length**	**Upper rec/tion length**	**Detac. upper**	**Reatt. upper**
Gartling [32]	12.200	11.260	9.700	20.960
Erturk [31]	11.830	11.070	9.470	20.553
Keskar [33]	12.190	11.250	9.710	20.960
Santos [1]	11.950	--	--	--
Lee [2]	12.700	--	--	--
Present work	12.500	11.050	9.830	20.880

Table 15: Validation of the present recirculation results for step 90 *deg a*nd $^{H}/_{H_{ref}} = 2$

Re	Lower wall recirculation length	
	Present work	**Erturk [31]**
100	2.340	2.922
400	7.420	8.237
800	12.500	11.834
1200	15.060	14.299
1700	16.240	16.917

As we can see by the following figures, no detection of recirculation is presented in very low *Re*, while the appearance of the upper bound recirculation depends on the *Re* values and the inclination angle as well (Fig. 6). The influence of the inclination angle is very clearly presented, showing that as you increase the value of the angle more recirculation length is expected according to the *Re* although the behavior of the fluids at the lower and at the upper wall is not the same (Fig. 7 and 8).

The sudden expansion, which takes place, cannot exist without the separation zones cost. However all the above results have been developed according to H_{ref} equal to 1 and therefore the above cases are dimensionless. Consequently according to the pipe hydraulic diameter as well as the inlet flow rate, the responsible engineer can choose the optimum combination in order to achieve the maximum expansion and the lower recirculation simultaneously. These findings are confirmed at the Fig. 6. Through these graphs the influence of the *Re* to the recirculation expansion is depicted for two values of the inclination angle. It seems that as more you increase the *Re* value as more the recirculation is developed for both of the pipes walls. Exactly the similar findings are concluded for all the other values of the inclination angle.

Interesting conclusions can be retrieved by Fig. 7 and 8, where the influence of the inclination step angle is presented to the recirculation expansion on both of the pipe walls. As it can be seen in the related figures, as the inclination angle increases for a constant *Re*, the recirculation length at the lower wall is increased in all of the cases, with more significant values at *Re* values 800, 1200 and 1700. This seems to be expected although maybe a higher increase should be addressed according to the flow rate changes. Our overall results seems to be compatible with Louda's ones [5], although he has studied inclined step flows for different *Re* values. Additionally, the lowest lengths are presented at the lowest *Re* values and the highest ones at the corresponded highest numbers.

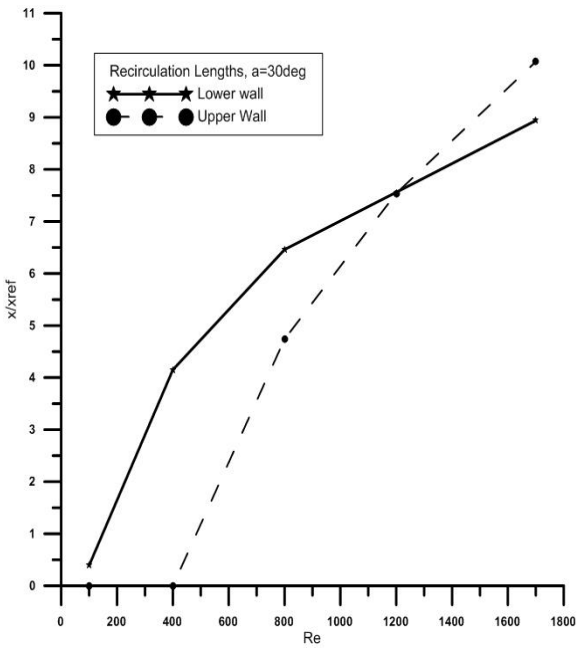

(a)

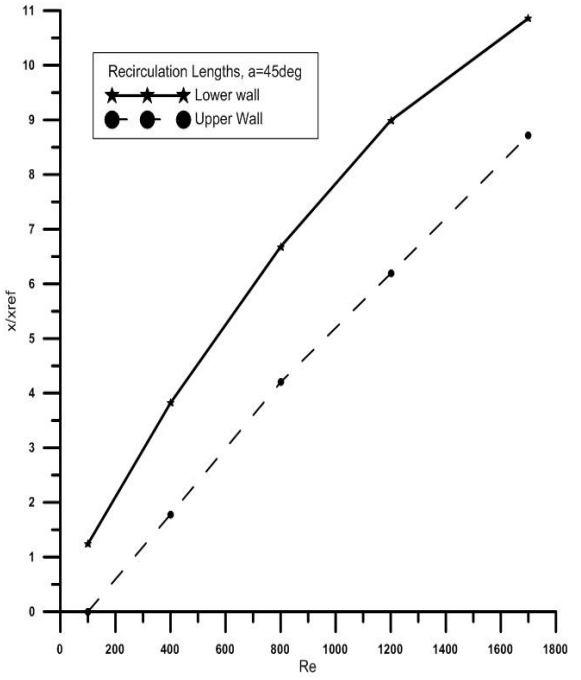

(b)

Fig. 6a, b. Inclination angle variation according to the *Re* values.

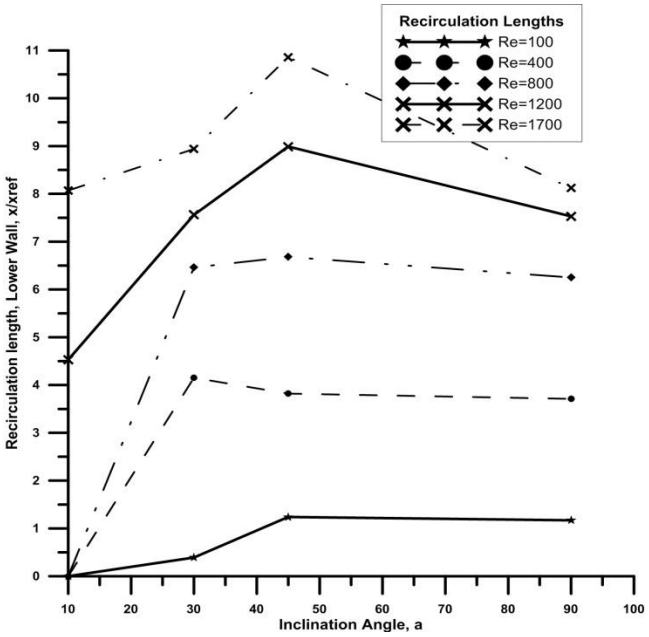

Fig. 7. Recirculation lengths at the lower wall of the pipe according to the inclination angle for various *Re.*

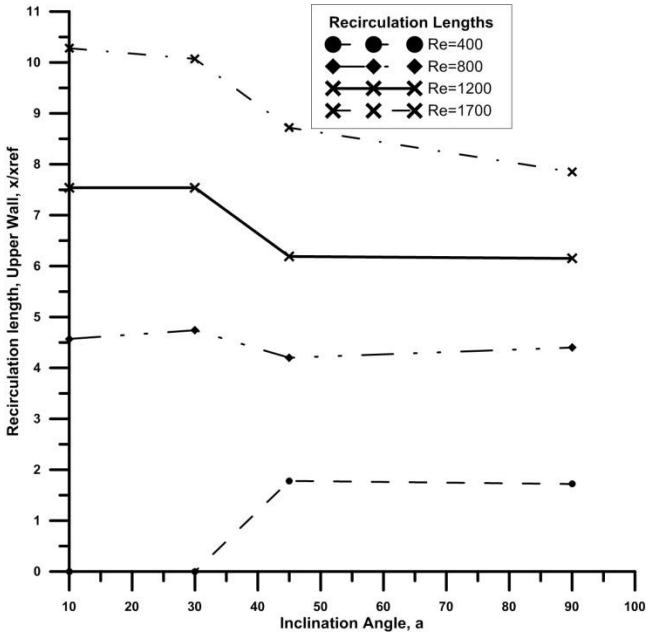

Fig. 8. Recirculation lengths at the upper wall of the pipe according to the inclination angle for various *Re* numbers.

However, the separation zones behavior is not the same at the upper wall of the pipes as at the lower ones. As we can clearly see in the Fig. 8, the more the inclination angle is increased the less extension of the upper wall recirculation is developed through the pipe, if we assume that the Re remains constant. However, again at the highest Re values, the more extended lengths are presented. It is important that this relationship is followed by the flow in all the various Re and by this way we may conclude that this relationship applies for all the range of Reynolds number of laminar flow.

Concerning the numerical procedure and the computational solution that it has been applied, it's worth mentioning that the CFL number is possible to receive high values for *Re* less than 1200. At the case of *Re* equal to 1700, many oscillations are appeared to the flow field if the CFL remains at high levels. Additionally in these cases the CPU time is sometimes huge or in some other cases no convergence of the flow field can be achieved. It is recommended for *Re* higher to 1300, the CFL to be less than 10, in order to achieve a stable and robust solution although in some cases the CPU time is much higher than was expected. However, in our numerical scheme, the dimensionless time step CFL can receive very high values, from 0.1 to 10000 and most of the times lead to a very fast convergence. These issues are expected due to the numerical technique nature in combination with the physical domain characteristics and aspect ratio values as these can be met in most of the numerical schemes, even the commercial ones [29,30].

By the other hand, important role for the convergence of the scheme is occurred by the number of dimensionless lengths of the pipe downstream of the step. It seems, after several test cases, that the *Re* value has a significant impact on this issue, as it was expected. For this reason, for the case of *Re* equal to 1700 more than 40 dimensionless lengths are needed (50 have been used), otherwise many oscillations are developed through the flow field and the convergence is almost impossible, even if the appropriate values of CFL and artificial compressibility term have been chosen.

However, as we have concluded after several test cases in this field, the channel length downstream of the step affects the quality and the accuracy of the numerical results as sometimes the flow field is converged without oscillations. In our future research the appropriate limits for this parameter requires further investigation, ensuring that every solution is length independent.

We agree with most of the researchers, who they claim that the entrance length of the pipe affects the numerical solution in low Re [31, 33]. According to

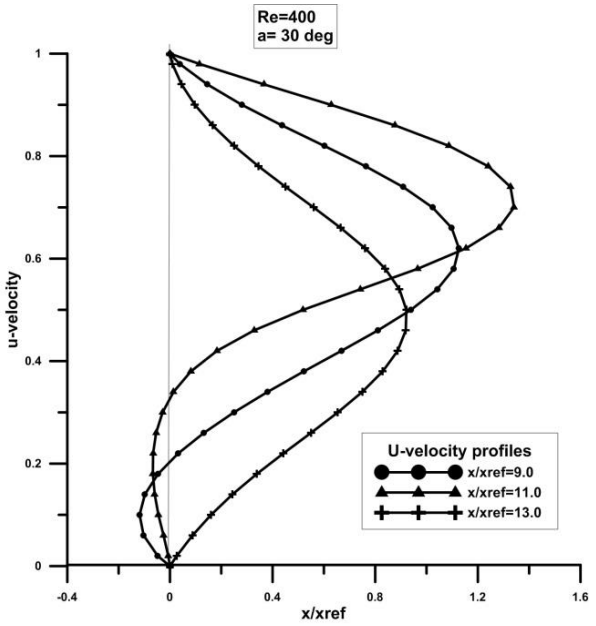

Fig. 9. Velocity profile along the pipe; a=30 deg and Re=400.

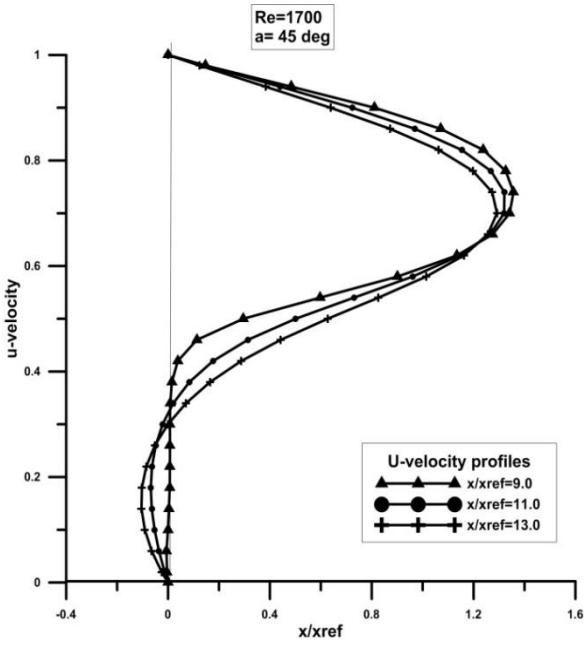

Fig 10. Velocity profiles; a=45 deg and Re=1700.

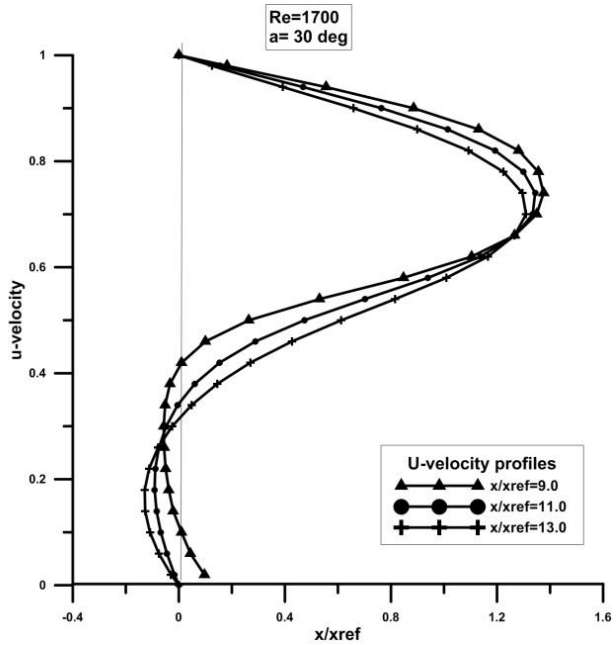

Fig. 11. Velocity profile along the pipe; angle=30 deg and Re=1700.

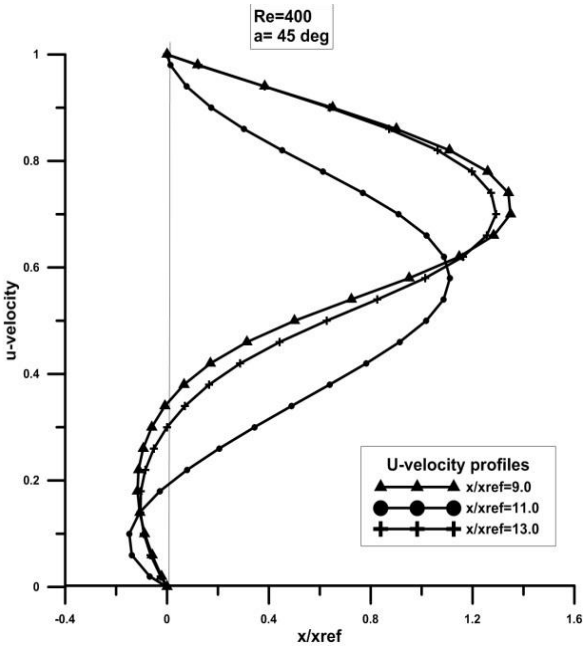

Fig. 12. Velocity profiles; a=45 deg and Re=400.

the literature an entrance length more than 6 dimensionless ones should be enough in order not to affect the flow distribution inside the pipe. In order to create an independent solution we have applied eight (8) lengths for the entrance pipe and it seems that there is no influence along the fluid flow field.

In fig. 9 to 12, the axial velocity profiles are presented for various *a* and *Re* values. As it was expected the profile is parabolic inside the pipe, while in the certain *x*-coordinate location the recirculation zones are depicted. It can be seen that the mass flow rate is conserved as well as the development of the flow is not affected by the downstream and upstream pipe's lengths.

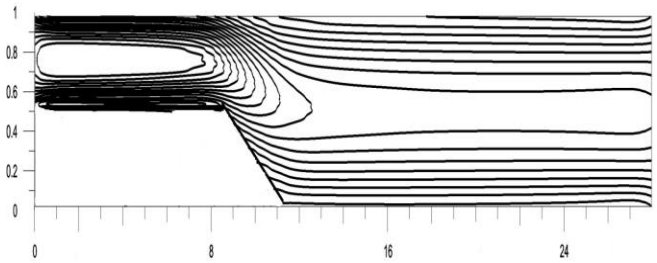

Fig. 13. Velocity contours along the pipe. Block nested grid, I=2, l=2. a=10^o and Re=100. No recirculation zone is detected.

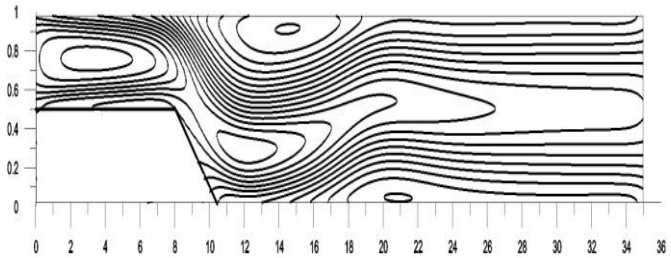

Fig. 14. Velocity contours along the pipe. Block nested grid, I=2, l=2. a=10^o and Re=1200. Very clearly are depicted upper and lower wall separation zones.

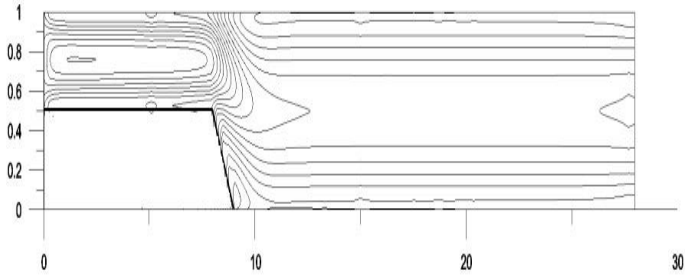

Fig. 15. Velocity contours along the pipe. Block nested grid, I=2, l=2. a=30^o and Re=100. Brief recirculation zone at the lower wall near to the step bound.

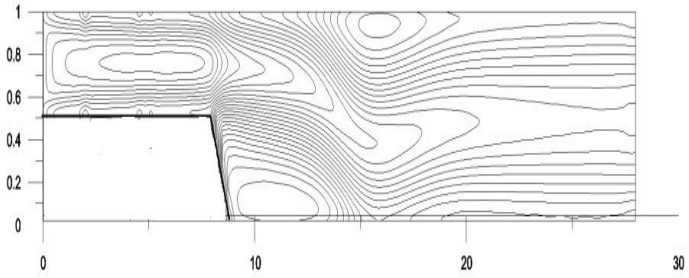

Fig. 16. Velocity contours along the pipe. Block nested grid, I=2, l=2, a=30^o and Re=800. Upper and lower wall separation zones. The lengths are close to each other.

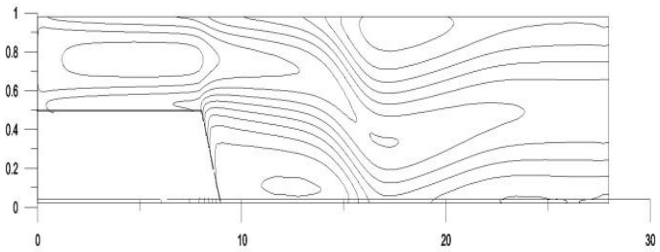

Fig. 17. Velocity contours along the pipe. Block nested grid, I=2, l=2. a=30^o and Re=1200. Very clearly are depicted upper and lower wall separation zones.

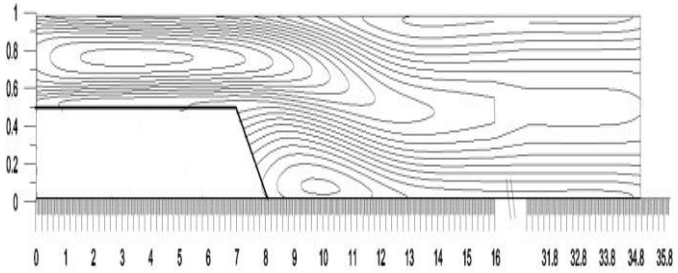

Fig. 18. Velocity contours along the pipe. Block nested grid, I=2, l=2. a=45^o and Re=400. Very clearly is depicted the lower wall separation zone.

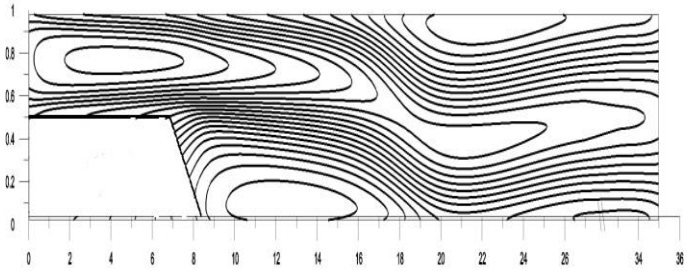

Fig. 19. Velocity contours along the pipe. Block nested grid, I=2, l=2. a=45^o and Re=1700. Extended recirculation on both of the bounds.

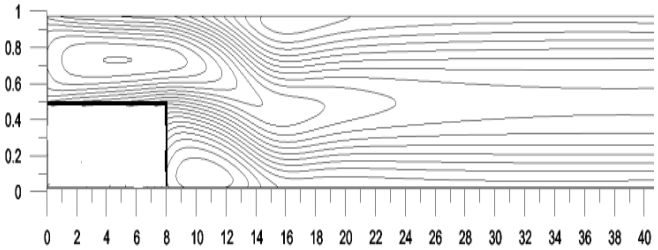

Fig. 20. Velocity contours along the pipe. Block nested grid, I=2, l=2. a=90^o and Re=800.

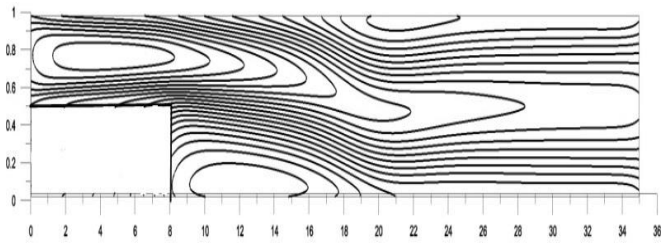

Fig. 21. Velocity contours along the pipe. Block nested grid, I=2, l=2. a=90^o and Re=1200.

In order to present the developing flow inside the pipes according to the different values of the angle *a*, providing more information concerning the recirculation zones, we present the above velocity contours for various *a* and *Re* values (Fig. 13 – 21). In Fig. 13 and 14 the flow distribution is presented when the inclination angle (*a)* is equal to 10 *deg*, with no recirculation for *Re*=100 and extended upper wall flow separation for *Re*=1200. In Fig. 15-17 velocity contours are presented for angle (*a*) equal to 30 *deg* where the separation zones are varied according to the *Re* values without any un-expectancy. The velocity contours for angle equal to 45 *deg* and 90 *deg* are finally presented in Fig. 18-21, providing certain details not only regarding the separation zones lengths but also for the related widths.

3.3 Block nested algorithm efficiency

Although a first validation attempt of our numerical method has been achieved through Tables 3-13, further investigation is needed in order to evaluate the efficiency of the proposed block nested grid algorithm to the aforementioned cases. For this purpose the computational estimation of the flows has been developed using various types of Cartesian grids, uniform and block nested ones with one (1) and two (2) levels of refinement. In the Tables 16 and 17 the used computational cells and the corresponded CPU time are presented for different grid types. By these data, it seems that using the block nested grid approach the CPU time is reduced significantly in some cases, more than 65%, maintaining constant and acceptable accuracy of the results. It's worth mentioning that the computational memory is decreased in every refined approach case in comparison with the corresponded uniform one.

Table 16: Computational cells and CPU time for various grid types and sizes; inclination angle a=30 deg.

Inclination angle a=30 deg		
Grid type and size	**No of cells**	**CPU time**
Re=400		
Uniform 651x26	14,980	531.24
Block Nested 321x13 I=2, l=1	4,849	190.00
Block nested 321x13 I=2, l=2	10,078	223.65
Re=800		
Uniform 651x26	14,980	518.00
Block Nested 321x13 I=2, l=1	4,849	205.15
Block nested 161x13 I=2, l=2	10,078	237.49
Re=1700		
Uniform 651x26	14,980	1067.72
Block Nested 321x13 I=2, l=1	4,849	426.48
Block nested 161x13 I=2, l=2	10,078	527.15

Table 17: Computational cells and CPU time for various grid types and sizes; inclination angle a=90 deg.

Inclination angle a=90 deg		
Grid type and size	**No of cells**	**CPU time**
Re=400		
Uniform 651x26	14,989	708.30
Block Nested 321x13 I=2, l=1	4,858	245.13
Block nested 161x13 I=2, l=2	10,089	337.18
Re=800		
Uniform 651x26	14,989	786.19
Block Nested 321x13 I=2, l=1	4,858	302.73
Block nested 161x13 I=2, l=2	10,089	393.26
Re=1700		
Uniform 651x26	14,989	1550.36
Block Nested 321x13 I=2, l=1	4,858	689.71
Block nested 161x13 I=2, l=2	10,089	932.65

However, the most significant reduction is presented on the CPU time values, which leads to the conclusion that the refinement technique is efficient enough

concerning the initial objectives and appropriate for the numerical solution of these flow fields.

4 Conclusions

The inclination angle effect to the recirculation zones and the behavior of the incompressible flow inside pipes is presented to the present paper with details. The flow characteristics, variables distribution, certain data infomration and points of upper and lower bound separation zones have been analytically presented for various values of *Re*. For the physical domain discretization we use Cartesian grids, despite of the non-Cartesian bounds existence and in order to overcome the huge amount of computational cells that are needed, in most of the cases, in order to receive the necessary fully developing flow, we develop a block nested refinement algorithm, which can be easily applied to the aforementioned flow domain. The artificial compressibility method has been applied for the numerical solution of the Navier-Stokes equations, while the appropriate way of the boundary conditions application has been studied according to each bound of the final discretized domain. It seems that if the *Re* is higher than 400 and less than 1700, two separation zones are developed inside the pipe in both of the bounds. The related detachment and reattachment points are clearly presented for every case and the final results show that in most of the cases the higher *Re* the more extended recirculation area for a certain inclination angle. The most interesting and useful conclusion is the influence of the inclination angle of the pipe to the separation zones, which seems to be not the same for both of the pipe's bounds. More specifically, as the inclination angle is increased, it seems that the recirculation length at the lower wall is increased as well, for all the range of *Re* values. It's worth mentioning, that our results have been validated for all the range of Re for various grid sizes uniform and ununiformed as well, either by the corresponded ones by the literature either by commercial software . By this way relating data are presented in order to prove the grid independence of our method as well as the validation and efficiency of the block nested algorithm with acceptable accuracy. It seems that the accuracy of the block nested algorithm is accepted while the CPU time can be reduced more than 50% in most of the cases according to the *Re* and the used refinement levels. Further research will be developed concerning the extension of the methodology to turbulent flows as well as to the study of the influence of the expansion ratio in similar pipes.

References

[1] Santos R., Oliveira K., Figueiredo J., Influence study of the entrance channel in a two-dimensional backward-facing step flow, Mecanica Computacional, vol. XXIX, pp. 3347-3358, 2010

[2] Lee T. and Mateescu D. Experimental and numerical investigation of 2-D backward-facing step flow. Journal of fluids and structures, vol. 12, pp. 703–716, 1998

[3] Armaly B., Durst F., Pereira J., and Schounung B. Experimental and theoretical investigation of backward-facing step flow. Journal of fluid mechanics, vol. 127, pp. 473–496, 1983.

[4] Manzan W., Vilela C., Mariano F., "Experimental and computational simulations of the flows over backward facing step", Proceedings of 22nd Int. COBEM2013, SP, Brazil

[5] Louda P., Prihoda J.,Kozel K.,Svacek P., "Numerical simulations of flows over 2D and 3D backward facing inclined steps", Int. Journal of heat and Fluid flow

[6] Louda P., Kozel K., Prijoda J., Benes L., Kopacek T., Numerical solution for incompressible flow through branched channel", Comput. Fluids, vol. 43, pp. 268-276, 2013

[7] Torres Maj., Garcia J., Numerical characterization of particle dispersion in the turbulent recirculation zones of sudden expansion pipe flows, Proceedings of the 6th European conference on computational Fluid dynamics, Barcelona, 2014

[8] Razavi S., Hosseinali M., A review of pressure behavior after a backward – facing step, Recent advances in Fluid Mechanics, pp. 52-58, 2009

[9] Kaiktsis L., Karniadakis G.E., and Orszag S.A. Onset of three-dimensionality, equilibrium, early

transition in flow over a backward-facing step. Journal of Fluid Mechanics, 501–528, 1991.

[10] Wallin S., Johansson A.V., " A complete explicit algebraic Reynolds stress model for incompressible and compressible turbulent flows", Journal Fluid Mechanics, vol. 403, pp.89-132

[11] Nassab S., Moosavi R., Sarvani S., " Turbulent forced convection flow adjacent to inclined forward step in a duct", Int. J. of Thermal Sciences, vol. 48, pp. 1319-1326, (2008)

[12] Coirier, W.J. and Powell, K.G., "An accuracy assessment of Cartesian-mesh approaches for the Euler equations", J. of Computational Physics, Vol. 117, pp. 121-131, 1995

[13] Georgantopoulou Chr.G., Pappou Th.J., Tsaggaris S.G., "Cartesian grid generator for N-S numerical simulation of flow fields in curvilinear geometries", Proceedings of the 4th GRACM congress on comput. Mechanics, pp. 526-534, 2002

[14] Wang, Z.J., "A Quadtree-based adaptive Cartesian/Quad grid flow solver for Navier-Stokes equation", Computers and Fluids, Vol. 27, pp.529-549, 1998

[15] Karai E., Kultari A., Haluk M., "Quad-tree based geometric – adapted Cartesian grid generation", Recent Advances in continuum Mechanics, Hydrology and Ecology, Vol. 1 pp. 15-25

[16] Agresar, G., Linderman J.J., Tryggvason, G. and Powell, K.G., "An adaptive, Cartesian, front-tracking method for the motion, deformation and adhesion of circulating cells", J. of Computational Physics, Vol. 143, pp. 346-380, 1998

[17] Phan H., Wen L., Zhang H., Numerical simulation and analysis of gas liquid flow in a T-junction micro channel, Advances in Mechanical Engineering, (2012), ID 231675.

[18] Iqbal S., Ansari A., Javed A., Siddiqui, "An adaptive Finite Element formulation for the solution of second order obstacle problems using quadratic lagrance polynomials", Journal of Numerical Analysis, industrial and applied Mathematics, vol.9-10, pp.37-45, 2016

[19] Georgantopoulou C., Georgantopoulos G., Vasilikos N., Numerical analysis and modeling of recirculating flows, Int. Journal of mathematical Models and Method in Applied Sciences, 9 (2015) 248-260.

[20] Tseng Y., Ferziger J., "A ghost-cell immersed boundary method for flow in complex geometry", J. of Computational Physics, vol.192, pp. 593-623, 2003

[21] Georgantopoulou C., Georgantopoulos G., Vasilikos N., Saw tooth approximation and numerical solution for flow in inclined channels, WSEAS Transactions on Fluid mechanics, 10 (2015) 69-79

[22] Chr.G. Georgantopoulou and S. Tsangaris, "Block mesh refinement for incompressible flows in curvilinear domains", Applied Mathematical Modeling,Vol.31, pp2136-2148.

[23] Berger M.J. and Collela P., "Local adaptive mesh refinement for shock hydrodynamics", J. of Comput. Physics, Vol. 83, pp.64-84, 1989.

[24] Pappou, Th. and Tsangaris, S., "Development of an artificial compressibility methodology using Flux Vector Splitting", International J. for Numerical Methods in Fluid, Vol. 25, pp.523-545, 1997

[25] Georgantopoulou Chr., Georgantopoulos G., Vasilikos N. and Tsangaris S., "Cartesian refinement grid generation and numerical calculation of flows around Naca0012 airfoil" Proceedings of Int. Conference on Applied mathematics, simulation, modeling, pp.256-263

[26] Mavromatidis, L., El Mankibi, M., Michel, P., Bykalyuk, A., & Santamouris, M. (2012). Guidelines to study numerically and experimentally reflective insulation systems as applied to buildings. Advances in Building Energy Research, 6, 2–35

[27] Mavromatidis, L., Michel, P., El Mankibi, M., & Santamouris, M. (2010). Study on Transient heat transfer through multilayer thermal insulation: Numerical analysis and experimental investigation. Building Simulation, 3, 279–294

[28] Biswas G., Breuer M., Durst, Backward-Facing Step Flows for Various Expansion Ratios at Low and moderate Reynolds Numbers, Transactions of ASME, vol. 126, pp. 362-374, 2004

[29] C. Georgantopoulou, Feras Ali, N. Vasilikos, G. Georgantopoulos, "Numerical modelling and investigation of crude oil flow in T-junction channels", Applied Mechanics and Materials, vol. 829, pp. 15-20, doi: 10.4028/www.scientific.net/AMM.829.15, 2016.

[30] Kanfoudi H., Zgoli R., (2015), "Modeling and computation of the cavitating flow in injection nozzle holes", Int. Journal of Modeling, Simulation and Scientific Computing, vol. 6, ID: 1550003

[31] Erturk E., (2008), "Numerical solutions of 2-D steady incompressible flow over a backward-facing step, part I: high Reynolds number solutions", Computers and Fluids, vol. 37, pp. 633-655.

[32] Gartling D., (1990), "A test problem for outflow boundary conditions – flow over a backward-facing step", Int. Journal Numerical methods, vol. 11, pp. 953-967.

[33] Barton Ie., (1997), The entrance effect of laminar flow over a backward-facing step geometry", Int. Journal Numerical methods Fluids, vol. 25, 663-644.